Evidence of Ba-rich surface segregation in $Ba_{1-x}Sr_xTiO_3$ and Ba-rich surfactant in $SrTiO_3$/ $Ba_{1-x}Sr_xTiO_3$ stacks grown by combinatorial pulsed laser deposition

Santiago Agudelo-Estrada[1*], *Nick* Barrett[1], *Christophe* Lubin[1], *Jérôme* Wolfman[2], *Beatrice* Negulescu[2], *Pascal* Andreazza[3], and *Antoine* Ruyter[4]

[1]SPEC, CEA, UMR 3680 CNRS, Université Paris-Saclay, F-91191 Gif-sur-Yvette, France
[2]GREMAN, UMR 7347 CNRS, Univ. de Tours, Parc de Grandmont, F-37200 Tours, France
[3]ICMN, UMR 7374 CNRS, Univ. d'Orléans, 1b rue de la Férollerie, F-45071 Orléans, France
[4]CRISMAT, UMR6508 CNRS, ENSICAEN, 6 Bd du Maréchal Juin, F-14050 Caen, France

Abstract. The interface of a $La_{0.7}Sr_{0.3}MnO_3/SrTiO_3$ bilayer was modulated by introducing 3 unit cells of $Ba_{1-x}Sr_xTiO_3$ using Combinatorial Pulsed Laser Deposition. A wide range of chemical compositions was studied within the same sample, with BSTx stoichiometry variable from 0.5 to 1 along Y-axis, while the SrTiO3 overlayer thickness was modified along the X direction [Fig. 1(a)]. We performed high-resolution, laboratory-based angle-resolved XPS studies of the BSTx film surface providing information on the thickness and composition of the surface and sub-surface layers. Based on the attenuation of the La 3d core-level photoemission signal from the $La_{0.7}Sr_{0.3}MnO_3$ bottom layer, the BST layer is 1.2 nm thick. XPS Ba $3d_{5/2}$ core-level spectra were acquired at positions corresponding to different nominal Ba/Sr stoichiometry. In all measurements, the Ba $3d_{5/2}$ core-level spectra can be represented by two main components, i.e. one component at higher binding energy (BE = 780.54 eV) corresponding to surface contribution and the other one at lower binding energy (BE = 778.92 eV) corresponding to sub-surface contribution (Figs. 2 and 3). Going from normal to 60° emission angle and using a 3-unit cell thick film model, the surface to sub-surface intensity ratio clearly evolves providing evidence of a Ba-rich surfactant. The surfactant effect is more significant for lower nominal Ba stoichiometry.

1 Introduction

The deployment of 5G technology has raised issues of energy consumption, reception quality, and call failure rate. All three can be minimized by continuously adjusting the antenna impedance. A voltage controllable impedance matching circuit with a highly tunable, ferroelectric (FE) capacitance is required. Voltage-tunable capacitors based on the perovskite ferroelectric solid solution $Ba_{1-x}Sr_xTiO_3$ (BSTx) have excellent tunability/losses compromise associated with an easily adjustable Curie temperature (via the Ba/Sr ratio), leading to a far better quality factor (i.e. low dielectric losses at GHz frequencies) than other competing technologies [1, 2]. Working at higher frequencies or lower voltage requires the reduction of the film thickness. In thin films (~50 nm), the formation of a non-FE, chemically distinct interface layer with altered dielectric properties and the increased leakage current can be detrimental to device performance [3]. The idea is to mitigate these limitations by the introduction of an interface control layer that allows manipulating the chemical bonding, promotes atomic rearrangement and possibly engineer better dielectric response. This requires detailed studies of the chemistry and electronic structure of the dielectric/BSTx interface.

2 Experimental

We have used combinatorial pulsed laser deposition to create a library of metal/semiconductor interface layers with continuous in-plane chemical modulation and thickness [4, 5]. We have grown a $La_{0.7}Sr_{0.3}MnO_3/Ba_{1-x}Sr_xTiO_3/SrTiO_3$ sample on a [001] oriented TiO_2 terminated $SrTiO_3$ (STO) substrate, shown schematically in figure 1, with the 3-unit-cell (approximately 1.2 nm) thick BSTx composition modulated along the sample ($0.5 \leq x \leq 1$). The $SrTiO_3$ overlayer thickness varies from 1.1 nm to 15.4 nm. The deposition conditions were: 650°C substrate temperature, 200 mTorr O_2 pressure and 1.6 J/cm² laser fluence. These deposition parameters promote 2D epitaxial growth of the layers, verified through intensity oscillation of Reflection High Energy Electron Diffraction spots before the sample fabrication. The BSTx interfacial layer was deposited from $Ba_{0.5}Sr_{0.5}TiO_3$ and

* Corresponding author: santiago.agudeloestrada@cea.fr

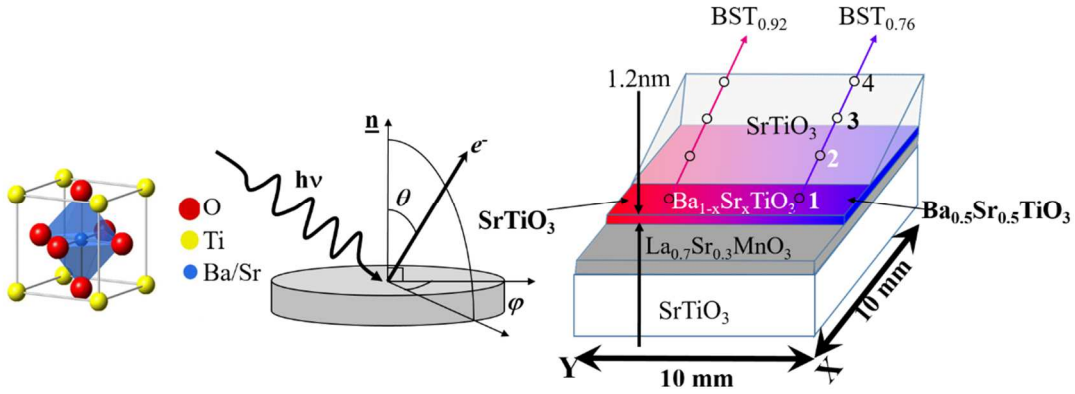

Fig. 1. Schematic of the ferroelectric STO/LSMO (22 nm)/BSTx (1.2 nm)/STO (1.1 nm – 15.4 nm) sample grown by combinatorial pulsed laser deposition and investigated with angle-resolved X-ray photoemission spectroscopy.

$SrTiO_3$ targets. In order to reduce carbon contamination on the surface, the sample was cleaned by short (5 minutes) exposure to ozone just before introduction into the XPS system, followed by annealing in vacuum at 300 °C for 15 min.

The XPS measurements were conducted using a monochromatic Al Kα source (1486.7 eV) and the spectra were recorded with an Argus-128 hemispherical analyzer (ScientaOmicron). The pass energy of 20 eV gave an overall resolution of 0.3 eV. The emission angle relative to the sample surface was varied in order to modulate the probing depth. The deconvolution of the core level spectra was performed using the CasaXPS software [6], and the backgrounds used were of the Shirley type. The peaks were modeled using a Voigt function, a convolution of Lorentzian and Gaussian functions.

3 Results

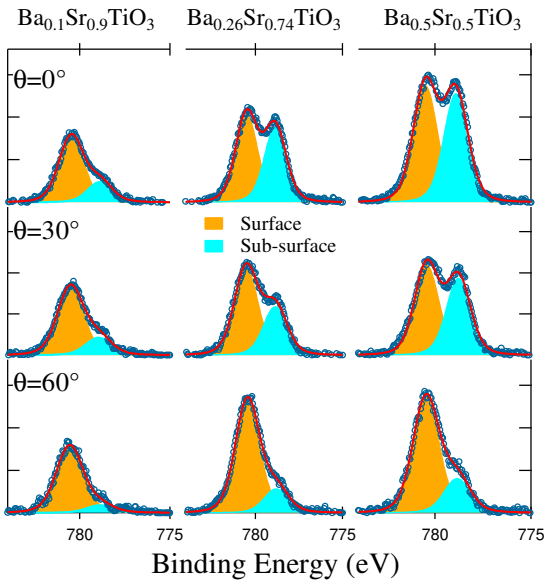

Fig. 2. Ba $3d_{5/2}$ core-level spectra at normal emission (top), 30° (middle), and 60° (bottom) emission angles were acquired for three different BSTx surface positions corresponding to different nominal stoichiometry, i.e. $BST_{0.9}$ (left), $BST_{0.74}$ (center), and $BST_{0.5}$ (right).

We performed high-resolution, laboratory-based XPS studies of the single crystal BSTx film and monocrystalline STO overlayer as a function of the emission angle providing information on the thickness and composition of the surface and sub-surface layers. La 3d and Ba $3d_{5/2}$ core level spectra were recorded. The expected 1.2 nm thickness of the BSTx layer was confirmed by the attenuation of the La photoemission signal from the LSMO bottom layer compared to the signal from the bare LSMO (not shown here).

Figure 2 compares Ba $3d_{5/2}$ core-level spectra acquired at three emission angles from the 1.2 nm thick BSTx layer for three different compositions, i.e. $BST_{0.9}$, $BST_{0.74}$, and $BST_{0.5}$, as a function of the emission angle. Analysis of these spectra reveals two main components: the peak at higher binding energy (BE = 780.54 eV) is characteristic of the surface environment while the peak observed at lower binding energy (BE = 778.92 eV) is characteristic of the sub-surface environment. The relative intensity of the two peaks depends on the probing depth of the analysis (i.e. emission angle) and the nominal Ba/Sr stoichiometry. In fact, the sub-surface Ba intensity becomes lower with respect to that from the surface Ba phase with decreasing probing depth (increasing emission angle) and is, therefore, proportional to the Ba enrichment with respect to the absolute stoichiometry of the underlying BSTx film. By changing the emission angle to 30° and 60°, increasing the sensitivity to the surface with respect to the sub-surface BSTx layer, we observe a relative Ba enrichment of the BSTx surface as compared to the sub-surface.

Table 1. Barium concentration depth profile.

Nominal Stoichiometry	Surface Stoichiometry	Sub-surfaces Stoichiometry
$Ba_{0.5}Sr_{0.5}TiO_3$	0.64	0.43
$Ba_{0.26}Sr_{0.74}TiO_3$	0.36	0.21
$Ba_{0.1}Sr_{0.9}TiO_3$	0.2	0.05

The quantitative analysis of the Ba $3d_{5/2}$ of the BSTx layer points to the segregation of Ba at the surface. Using a 3-unit-cell thick film model (1.2 nm), the ratio of surface intensity to sub-surface [Eq. (1) and (2)] and assuming that the global mean stoichiometry of the 3 layers is the

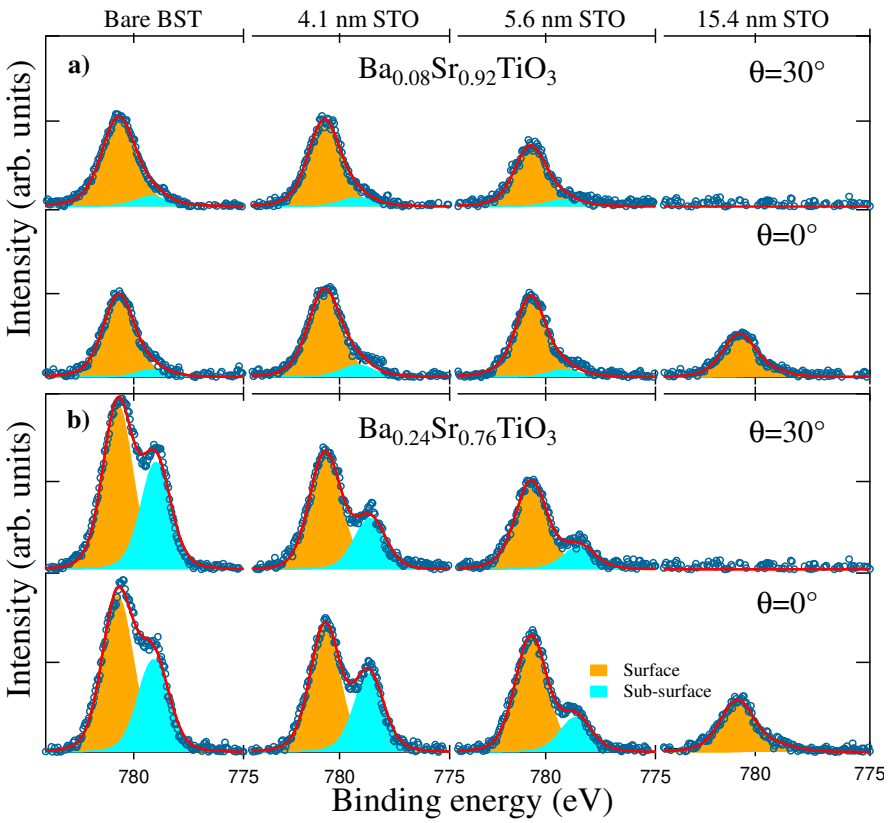

Fig. 3. Ba $3d_{5/2}$ core-level spectra at normal emission (bottom), and 30° (top) emission angles were acquired at four different STO overlayer thicknesses (increases from left to right) at fixed nominal stoichiometry, i.e. (a) $BST_{0.92}$, and (b) $BST_{0.76}$

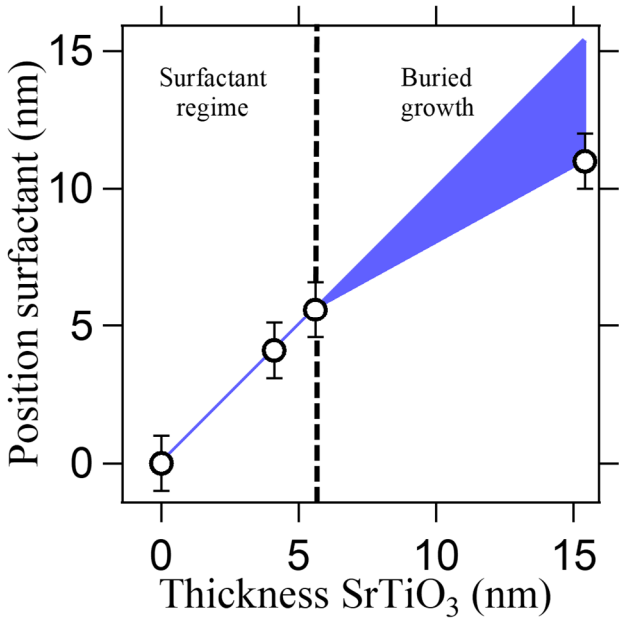

Fig.4. The surfactant position as a function of STO thickness. The suggested dielectric/ferroelectric growth model interface presents a surfactant regime (left) and a buried growth (right).

nominal one; we calculate the barium concentration depth profile [Table (1)]

$$\frac{I_{Surface}}{I_{Sub-surface}} = \frac{Surface\ conc.}{Sub-surface\ conc.(k+k^2)} \quad (1)$$

$$k = exp\left(-\frac{0.4\ nm}{\lambda_{IMFP}\cos\theta}\right) \quad (2)$$

where λ_{IMFP} is the inelastic mean free path of Ba 3d electrons in BSTx And k is the single layer attenuation factor [7]. Its value of 1.5 nm was calculated using the

Tanuma, Powell, and Penn (TPP-2M) algorithm, implemented in the QUASES-IMFP-TPP2M software.

To evaluate the Ba-rich surfactant effect, we performed XPS as a function of the STO overlayer thickness for two different emission angles. Ba $3d_{5/2}$ core-level spectra were recorded. Figs. 3(a) and 3(b) compares the normalized Ba $3d_{5/2}$ core-level spectra from different positions corresponding to four distinct STO thicknesses (0 nm, 4.1 nm, 5.6 nm, and 15.4 nm) at two nominal Ba/Sr stoichiometries, i.e. $BST_{0.92}$ and $BST_{0.76}$.

The most striking feature is the persistence of significant Ba 3d signal up to at least 5.6 nm STO and, in the case of normal emission, up to the thickest STO layer; this is the signature of Ba segregation to the surface of STO, i.e. the formation of a chemically distinct surfactant. Given the estimated inelastic mean free path of 1.5 nm, in the absence of a surfactant effect, we would expect near complete extinction of the Ba 3d emission for 4.1 nm STO overlayer. Instead, the intensity remains comparable to that observed for the bare BST, i.e. there is both Ba segregation at the STO surface and Ba enrichment with respect to the nominal stoichiometry of the underlying BST film.

Analysis of these spectra reveals that the surfactant effect is present up to 5.6 nm. Even for 15.4 nm STO overlayer there is a weak Ba 3d signal at normal emission for both nominal BST stoichiometries. Recalling that the 3λ probing depth is ~ 4.5 nm, we can deduce that the Ba-rich surfactant only starts to be covered by the STO for STO thicknesses ≥ 10 nm. This is important information, as thin dielectric layers are often used to modify the electrical boundary conditions, to engineer the depolarizing field or to create diffusion barriers in capacitor or gate stacks.

In Figure 4, we plot the surfactant layer position above the BST film as a function of the STO thickness, assuming that the surfactant layer truly floats on the STO and does not dissipate or dilute into the STO during growth. The surfactant regime ranges from 0 nm to at least 5.6 nm, possibly more. The surfactant layer starts to be buried at higher STO coverages and is ~ (11 ± 1) nm above the BST film at the end of the STO growth, i.e. buried under 4.5 nm of STO. The driving force behind the Ba surfactant effect may be the epitaxial strain exerted by the STO substrate through LSMO and BSTx layers. Ba effective ionic radii $\left(Ba_{XII}^{2+} = 1.61\text{Å}\right)$ is much bigger than Sr $\left(Sr_{XII}^{2+} = 1.44\text{Å}\right)$ [8] leading to bigger lattice parameters for BSTx compared to STO. Surface Ba with dangling bounds helps reducing the strain, as does Ba atoms progressive dilution into STO matrix.

4 Conclusion

Angle-resolved XPS measurements were performed to measure the surface and sub-surface stoichiometry in a stack suitable for integration into a BSTx based capacitor. We provide evidence of the Barium-rich surfactant effect in BSTx thin films deposited by CPLD. The Ba segregation is stronger for lower nominal Ba/Sr stoichiometry.

A 3-unit-cell thick film model and the ratio of surface intensity to sub-surface obtained by XPS allowed us to calculate the Barium concentration depth profile. The enrichment of Ba content at the surface as compared to the sub-surface may be associated with strain release in the BST epitaxially grown following the smaller lattice parameter of the STO substrate. In addition to the changes in local chemistry, the induced strain gradients may also alter the electrical properties of the BST film, potentially reinforcing local polarization and ferroelectric properties via flexoelectric effect [9].

This project has received funding from the Agence Nationale de la Recherche under Grant No. ANR-20-CE24-0008-BePolar.

References

1. P. Bao, T. J. Jackson, X. Wang, M. J. Lancaster, J. Phys. D: Appl. Phys. **41** 063001 (2008)
2. M. P. J. Tiggelman, K. Reimann, F. Van Rijs, J. Schmitz, R. J. E. Hueting, IEEE Trans. Electron Devices. **56**, 2128-2136 (2009)
3. M. Stengel, D. Vanderbilt, N. Spaldin, Nat. Mater. **8**, 392–397 (2009)
4. C. J. M. Daumont, Q. Simon, E. Le Mouellic, S. Payan, P. Gardes, P. Poveda, B. Negulescu, M. Maglione, J. Wolfman, J. Appl. Phys. **119**, 094107 (2016)
5. J. Wolfman, B. Negulescu, A. Ruyter, N. Niang, N Jaber, Practical Applications of Laser Ablation (2020)
6. N. Fairley, see http://www.casaxps.com/ for complete documentation of fit procedure (2020)
7. L. Q. Zhu, N. Barrett, P. Jégou, F. Martin, C. Leroux, E. Martinez, H. Grampeix, O. Renault, A. Chabli, J. Appl. Phys. **105**, 024102 (2009)
8. R. D. Shannon, Acta Cryst. **A32**, 751-767 (1976)
9. P. Zubko, G. Catalan, A. K. Tagantsev, Annu. Rev. Mater. Res . **43**, 387-421 (2013)